

Hybrid polymer networks of carbene and thiol ene

Djordjevic, Ivan; Wicaksono, Gautama; Singh, Juhi; Singh, Manisha; Ellis, Elizabeth G. ; Alraddadi, Maher; Dove, Andrew; Steele, Terry W. J.

DOI:

[10.1016/j.eurpolymj.2022.111502](https://doi.org/10.1016/j.eurpolymj.2022.111502)

License:

Creative Commons: Attribution-NonCommercial-NoDerivs (CC BY-NC-ND)

Document Version

Peer reviewed version

Citation for published version (Harvard):

Djordjevic, I, Wicaksono, G, Singh, J, Singh, M, Ellis, EG, Alraddadi, M, Dove, A & Steele, TWJ 2022, 'Hybrid polymer networks of carbene and thiol ene', *European Polymer Journal*, vol. 178, 111502. <https://doi.org/10.1016/j.eurpolymj.2022.111502>

[Link to publication on Research at Birmingham portal](#)

General rights

Unless a licence is specified above, all rights (including copyright and moral rights) in this document are retained by the authors and/or the copyright holders. The express permission of the copyright holder must be obtained for any use of this material other than for purposes permitted by law.

- Users may freely distribute the URL that is used to identify this publication.
- Users may download and/or print one copy of the publication from the University of Birmingham research portal for the purpose of private study or non-commercial research.
- User may use extracts from the document in line with the concept of 'fair dealing' under the Copyright, Designs and Patents Act 1988 (?)
- Users may not further distribute the material nor use it for the purposes of commercial gain.

Where a licence is displayed above, please note the terms and conditions of the licence govern your use of this document.

When citing, please reference the published version.

Take down policy

While the University of Birmingham exercises care and attention in making items available there are rare occasions when an item has been uploaded in error or has been deemed to be commercially or otherwise sensitive.

If you believe that this is the case for this document, please contact UBIRA@lists.bham.ac.uk providing details and we will remove access to the work immediately and investigate.

1 **Hybrid polymer networks of carbene and thiol ene**

2 Ivan Djordjevic¹, Gautama Wicaksono¹, Juhi Singh^{2,3}, Manisha Singh¹, Elizabeth G. Ellis¹,
3 Maher A. Alraddadi⁴, Andrew P. Dove⁴ and Terry W.J. Steele¹

4

5 ¹School of Materials Science and Engineering (MSE), Nanyang Technological University,
6 Singapore 639798.

7 ²School of Chemical and Biomedical Engineering, Nanyang Technological University,
8 Singapore 637457.

9 ³NTU Institute for Health Technologies, Interdisciplinary Graduate Program, Nanyang
10 Technological University (NTU), Singapore 637335.

11 ⁴School of Chemistry, University of Birmingham, Edgbaston, Birmingham B15 2TT, United
12 Kingdom

13 *Corresponding author: Terry W. J. Steele (e-mail: wjsteele@ntu.edu.sg)

14

15

16

17

18

19

20

21

22

23

24

ABSTRACT

Thiol/ene-based resorbable elastomers display tough elongation but lack adhesion to soft tissues. Carbene-based bioadhesives (e.g. CaproGlu) allow soft tissue adhesion, but the covalent crosslinks limit extensibility after photoactivation. Herein thiol/ene resorbable elastomers are combined with a carbene bioadhesive into a 3-component hybrid network by exploiting tunable photoactivation of each macromolecule independently or simultaneously. Dual crosslinking was monitored by photorheometry, where 405 nm initiates formation of a thiol/ene elastomeric network, followed by 365 nm activation of diazirine-grafted polycaprolactone tetrol (CaproGlu). Dynamic shear moduli, gelation point, elongation at break, and lap shear stress of the hybrid polymer network are evaluated with respect to absorbed light energy dose. Surface-exposed unreacted CaproGlu enables adhesion of the hybrid network to various substrates, as well as intermolecular crosslinking within the transparent matrix. The network morphology and functional group conversion is evaluated through scanning electron microscopy and infrared spectroscopy, respectively. For the first time, we demonstrate hybrid thiol/ene/diazirine double sided bioadhesives with tunable dynamic moduli in the range of 10-800 kPa and 160 kPa lap-shear adhesion strength.

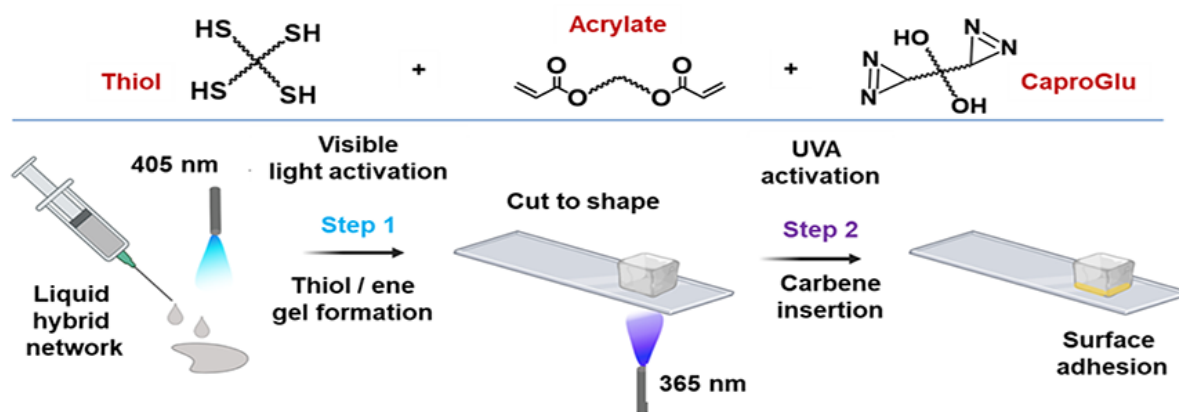
Keywords: *Hybrid polymer network, diazirine-grafted polycaprolactone; light curing; crosslinked elastomer; double sided adhesive.*

58 1. INTRODUCTION

59 Hybrid polymer networks consist of two or more entangled polymers which homogeneously
60 build the polymer system by physical and/or covalent crosslinks [1]. The strategy of
61 combining the properties of individual polymers could result in precise tuning of hybrid
62 material for targeted applications [2]. One of the obvious examples of hybrid networks are
63 “interpenetrated polymer network” (IPN) systems that have pushed the limits of what is
64 capable for viscoelastic elastomers, such as elongation that exceeds 2000% and resilience that
65 is unmatched with typical rubber networks [3]. Hybrid IPN materials can be produced both in
66 hydrogel [4] or solvent free forms [5]. Careful selection of the type of crosslinking chemistry
67 provides the strategy of design and control over unique material performance characteristic to
68 hybrid polymer networks [6]. In applications such as wound management, tissue sealing and
69 reconstruction, tissue adhesion plays a significant role. There are a number of hybrid
70 materials reported to adhere to tissues. Recent examples include allyl-functionalized
71 branched polymers mixed with tri-thiol crosslinking component [7], *in situ* forming multi-
72 monomer acrylate IPN hydrogel tissue patch [8], polyacrylamide/alginate hybrid hydrogels
73 [9] and two-component adhesive, composed by two different *p*-hydroxyphenyl-grafted
74 polymers: chitosan and polyethylene glycol (PEG) activated by hydrogen peroxide and
75 horseradish peroxidase [10]. Most of the bioadhesive systems (single components or hybrid
76 network) rely on interfacial bonding realized by acrylate crosslinking and are either limited to
77 topical use (i.e. cyanoacrylate) [11] or result in low adhesion strength (i.e. IPN hydrogels;
78 adhesion strength ~20 kPa) [8]. Another type of tissue adhesion is by physical interaction (i.e.
79 hydrogen or ionic bonds) where adhesion strength could be compromised by hydrolysis or
80 changes in local pH values [12]. Current unmet clinical needs require bioadhesives that
81 deviate from 2-part chemical curing designs. One-pot stimuli-sensitive crosslinking systems
82 are sought with specific design parameters, such as: (i) solvent-free liquid resins; (ii) benign
83 light activation energy that would yield rapidly gelling biomaterials; (iii) improved
84 crosslinking chemistry to provide model systems for investigations of hybrid network
85 adhesives. On-demand materials are sought for tissue adhesives with sufficient
86 adhesive/cohesive strength to replace mechanical fixation methods based on sutures or
87 staples.

88 Using activated esters presents another strategy for interfacial covalent bonding between
89 hybrid adhesive and surface amines on tissue substrates [13-15]. Although some important
90 advances have been made in the field with N-hydroxysuccinimide (NHS)-grafted

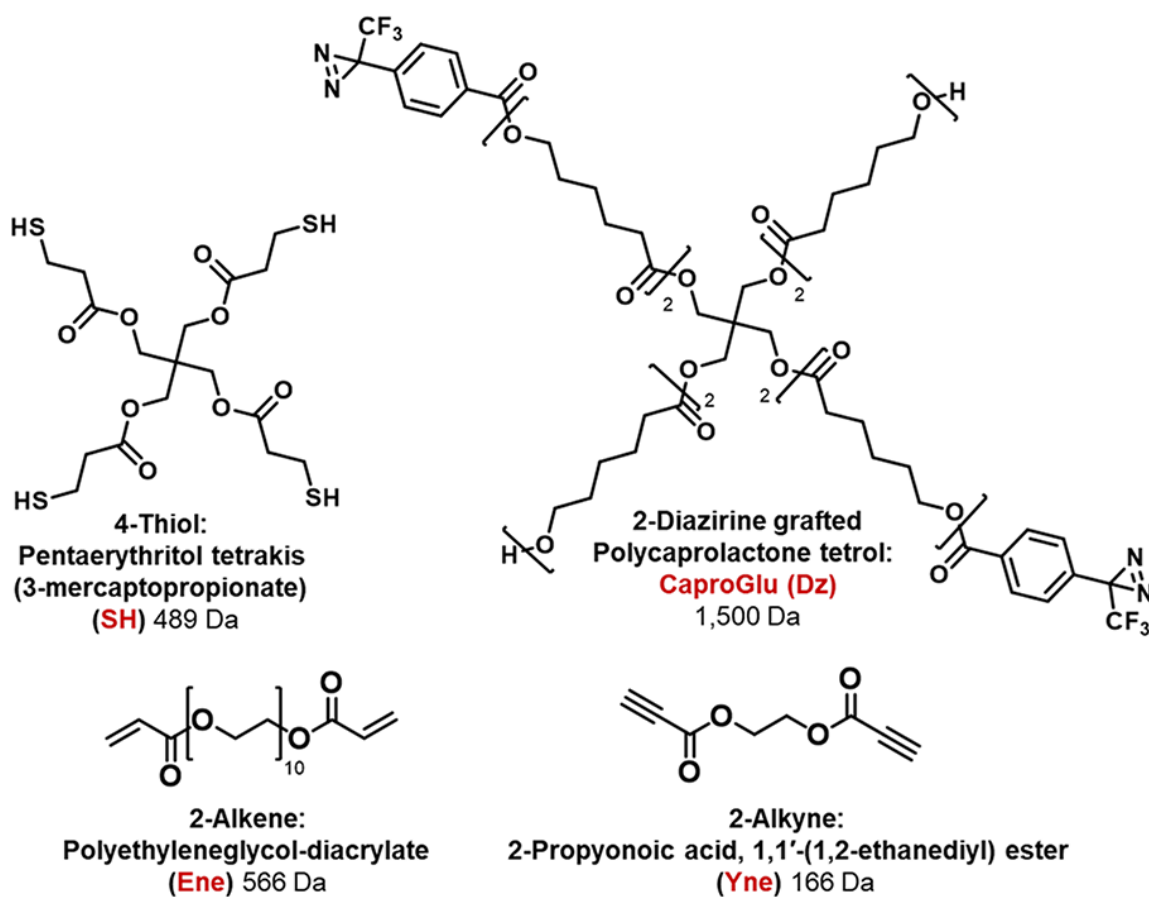
91 biomaterials, it should be noted that adhesion strength is dependent on concentration of
 92 surface amines that can vary for different tissues, causing modulation in adhesive
 93 performance [16]. Another potential drawback of NHS grafting technology is that requires
 94 dehydrated tissue prior to adhesive interaction, which often includes relatively complicated
 95 macromolecular designs [12, 13]. Carbene-based bioadhesives are under development to
 96 surpass current limitations of commercial tissue adhesives. Diazirine-grafted
 97 polycaprolactone polyol (CaproGlu) [17] was designed to be solvent-free liquid precursor for
 98 rapid light-induced gelation (both visible and UV light) and to be miscible with organic
 99 additives [18]. The hydrophobic nature of liquid CaproGlu allows solvent-free dissolution of
 100 other hydrophobic liquid polymers to yield hybrid network. Herein, CaproGlu's miscible
 101 nature is exploited to dissolve thiol/alkene and thiol/alkyne precursors into hybrid polymer
 102 network (**Figure 1**).



103
 104 **Figure 1.** 3-component double sided adhesive hybrid polymer network design by solvent-free
 105 mixture of (top), 4-functional thiol, PEG-diacrylate and diazirine-grafted polycaprolactone
 106 tetrol (CaproGlu); (bottom) syringable hybrid network undergoes liquid-to-solid transition
 107 upon activation with visible light (405 nm – Step 1) followed by diazirine-to-carbene
 108 activation (UVA light at 365 nm – Step 2) that results in interfacial covalent attachment of
 109 adhesive gel with solid surface.

110
 111 Polyethylene glycol-diacrylate (Ene), pentaerythritol tetrakis (3-mercaptopropionate) (SH), 2-
 112 propynoic acid, 1,1'-(1,2-ethanediyl) ester (Yne) and diazirine-grafted polycaprolactone tetrol
 113 (CaproGlu; abbreviated to “Dz” for diazirine functional groups) are mixed into hybrid
 114 networks that result in both single-step activation with polychromatic light in the range of
 115 320-500 nm (SH/Yne/Dz) and dual-step activation by monochromatic 405 nm light followed

116 by UVA activation (365 nm) for SH/Ene/Dz. The general hypothesis is that thiol/ene reaction
 117 results in liquid-to-gel transition upon exposure to visible light (405 nm; Step 1) where
 118 diazirines are stable. This 3-component hybrid gel can be formed in any desirable shape/size
 119 prior to diazirine-to-carbene reaction, activated by UVA light (365 nm; Step 2;). The carbene
 120 subsequently inserts into any type of solid surface resulting in covalent adhesion of
 121 crosslinked hybrid network. The simple blending procedure of components with different
 122 molecular geometries (**Figure 2**) provide a facile preparation method of injectable synthetic
 123 biomaterials with a wide range of elastic moduli possible [19].



133 radical reactions are light-activated in the presence of photoinitiator with controlled
134 crosslinking kinetics [22]. This crosslinking reaction is particularly useful for acrylate
135 systems in coatings industry, dental and tissue engineering applications [23, 24]. *In-situ* light
136 activation with visible light or with UVA light (i.e. absorbed light energy dose: 10-20 J) is a
137 polymerization method of choice for synthetic implant design where the implant first takes
138 shape/size of surgical site (Step 1) and subsequently adheres to solid substrate (Step 2;
139 **Figure 1**). For the first time, this paper describes diazirine-based 2-step crosslinked hybrid
140 polymer network with characteristics of double sided adhesive gel and controlled dynamic
141 mechanical modulus.

142

143 **2. EXPERIMENTAL SECTION**

144 **2.1 Materials**

145 Polyethyleneglycol-diacrylate (Ene; **Figure 2**), diphenyl (2,4,6-trimethyl benzoyl) phosphine
146 oxide (TPO) and other reagents and solvents (KOH, KMnO₄, HCl, MgSO₄, 1,1-
147 carbonyldiimidazole (CDI), deuterated and pure dichloromethane (DCM), diethyl ether;
148 Et₂O) are purchased from Sigma (Singapore). Pentaerythritol tetrakis (3-mercaptopropionate;
149 SH; **Figure 2**), 4-[3-(Trifluoromethyl)-3H-diazirin-3-yl] benzyl alcohol (Dz-MeOH) and 2-
150 Propynoic acid, 1,1'-(1,2-ethanediyl) ester (Yne; **Figure 2**) are purchased from TCI
151 Chemicals (Japan). Polycaprolactone tetrol (PCLT; M_w = 1000 Da) is kindly donated by
152 Ingevity (Capa™ 4101; Lot No. HTX06P024).

153 **2.2 Synthesis and preparation of 2-step light-activated hybrid polymer networks: thiol, 154 acrylate and diazirine-grafted polycaprolactone tetrol**

155 CaproGlu is diazirine-grafted PCLT (**Figure 2**) synthesized by previously published method
156 [25]. In brief, diazirine grafting is obtained by esterification reaction between PCLT and 4-[3-
157 (Trifluoromethyl)-3H-diazirin-3-YL] benzoic acid (Dz-COOH produced by Dz-MeOH
158 oxidation) conducted with 1,1- carbonyl diimidazole (CDI) used as a coupling agent. The
159 molar ratio of Dz-COOH/PCLT = 2/1 is deliberately chosen to yield ~50% diazirine
160 conjugation. Hybrid polymer networks: Yne/Ene/SH/CaproGlu are prepared by mixing liquid
161 components (**Figure 2**) in predetermined concentrations into glass vials; 2-component
162 mixtures (SH/Yne and SH/Ene) and pure CaproGlu (Dz) are used as controls for crosslinking
163 method in photorheometry experiment (**Table 1**). The solvent (DCM) is added to the mixture

164 (approximately up to 10% w/v polymer/solvent) and vortexed 3 times (20 sec each time).
 165 Stock solution of TPO (10% w/v; DCM) is added (maximum 0.1% w/w TPO/polymer) to the
 166 polymer solution and vortexed again 3 times (20 sec each time). The solvent is evaporated
 167 under vacuum to produce solvent-free hybrid polymer blends in the molar ratios displayed in
 168 **Table 1** (number of mmols of SH, Yne and Ene are normalized to CaproGlu set as 1 mmol).
 169

Table 1. Molar ratios of hybrid networks with controls normalized to CaproGlu concentration (pure CaproGlu is used as Control-1 in all measurements) and light activation methods: 405 nm and 365 nm are two consequent activation steps used in dual curing photorheology experiment.

Hybrid network composition	4-Thiol (SH)	2-Alkyne (Yne)	2-Alkene (Ene)	2-Diazirine (CaproGlu)	Light activation		
					320-500 nm	405 nm	365 nm
CaproGlu (Control-1)	-	-	-	1	x	√	√
SH/Yne (Control-2)	1	1	-	-	√	x	x
SH ₂ /Yne ₂ /Dz	2.3	2.3	-	1	√	x	x
SH/Ene (Control-3)	1	-	2	-	x	√	√
SH ₂ /Ene ₂ /Dz	2.0	-	2.2	1	x	√	√
SH ₁ /Ene ₂ /Dz	1.1	-	2.1	1	x	√	√
SH ₁ /Ene _{1.5} /Dz	1.1	-	1.5	1	x	√	√

170

171 2.3 Photorheometry analysis of hybrid polymer networks

172 Samples are analysed with Anton Paar MCR302 rheometer (SH/Yne/Dz: PP08 / 8 mm
 173 diameter probe / 0.2 mm probe-base gap) and MCR302 rheometer (SH/Ene/Dz: PP10 / 10
 174 mm diameter probe; 0.1 mm probe-base gap), equipped with UV-transparent glass base. The
 175 following is an example of rheometry evaluation: rotational shear at 10 Hz for 30 seconds,
 176 followed by dynamic shear for 120 seconds (1% amplitude; 10 Hz frequency) together with
 177 photoirradiation (UV light; OmniCure Series 1500 UV Spot Curing System with 320-500 nm
 178 bandpass filter (100 mW.cm⁻²) for 200 seconds (SH/Yne/Dz). Dual crosslinking (SH/Ene/Dz)
 179 is performed with two different light sources: each 3-component network and controls (**Table**
 180 **1**) are first subjected to rotational shear at 10 Hz for 60 seconds, followed by dynamic shear
 181 (1% amplitude; 10 Hz frequency) during which the samples are irradiated with 405 nm
 182 exposure (power: 100 mW.cm⁻²; Thorlabs SOLIS-405C High-Power LED), followed by 365
 183 nm UVA exposure (Convoy S2+ 365 nm Nichia UV Waterproof LED Flashlight; 100

184 mW.cm⁻²). Light diodes are calibrated with IL 1400 Radiometer. Storage (G') and loss (G'')
185 moduli are recorded over time during the dynamic shear. G' and G'' are measured both as a
186 function of irradiation time and energy (J.cm⁻²; referred to as "J" further in text).

187 **2.4 Fourier-transform Infrared Spectroscopy (FTIR) analysis**

188 FTIR spectra of 3-component hybrid networks (crosslinked by exposure to ambient light for
189 24 h) and pure CaproGlu are recorded before and after UVA activation (single components:
190 SH, Ene and CaproGlu are recorded as controls). Solid hybrid network sample is centred
191 between 2 UVA diodes (Supplementary Information; **Figure S1-2**) and activated from both
192 sides (10 J each side). Liquid samples (pure components) are placed on glass slides and
193 activated with 10 J dose of UVA light. FTIR spectra are recorded before and after UVA
194 activation in attenuated total reflection (ATR) mode at the following timepoints: before UVA
195 (neat), immediately after UVA activation and 10 min, 20 min, 30 min and 24 h post-UVA.
196 FTIR spectroscopy experiment is performed using PerkinElmer Frontier IR equipped with
197 ATR sampling accessory. Spectra are recorded over accumulation of 8 scans at resolution 4
198 cm⁻¹, at range of 4000-600 cm⁻¹. The theoretical calculation of the concentration of diazirine
199 groups, contained at 1 cm² surface with 1 μm thickness is performed by using the estimated
200 molecular weight of CaproGlu (1,500 Da) and the density of hybrid network determined
201 directly by weighing the samples with measured dimensions (**Table S2**).

202 **2.5 Scanning electron microscopy analysis of crosslinked hybrid polymer network:** 203 **cross-section morphology profile**

204 Crosslinked hybrid network is prepared by the same method as for FTIR spectroscopy and
205 lap shear adhesion experiments (10 J of absorbed light energy from each side of the square
206 sample (**Supplementary Video_1**) is cut in cross-sections and analysed with SEM. Samples
207 are subjected to platinum coating (90 s, chamber pressure <5 Pa at 20 mA). Images are
208 obtained by JSM 6360 SEM at an acceleration voltage of 5–20 kV and a working distance of
209 ~15 mm.

210 **2.6 Adhesion strength analysis of hybrid networks on polymer surfaces**

211 3-Component polymer networks in predetermined concentrations (**Table 1**) are casted into
212 petri dishes and irradiated with 405 nm diode for the total dose of 4 J. The samples are left to
213 crosslink for 24 h under ambient conditions to produce ~1 mm thick films for peel test
214 (**Figure S3**). Samples are placed on collagen film fixed with cyanoacrylate onto glass slide.

215 The sample is placed onto a collagen surface with one collagen film on the top of the sample
216 thus forming collagen/HPN/collagen sandwich structure (**Figure S4**). Both glass slides with
217 fixed collagen film (bottom surface) and the collagen strips (top surface) are soaked in
218 purified water followed by removal of excess water with lint free paper. The sample is fixed
219 with an additional glass slide (from the top) with the aid of paper clips (**Figure S4**). The
220 sample is irradiated with UVA (365 nm) light from both sides with the total dose of 20 J (10 J
221 from each side). After UVA activation, the paper clips and the glass slide from the top are
222 removed. The sample is mounted onto a peel test cell and the top collagen film is pulled
223 upwards to record the peel strength (N/m) vs displacement (mm). Each HPN composition as
224 well as CaproGlu control are measured with Series Force Measurement System (Chatillon
225 Force Measurement Products, USA) equipped with 100 N loading cell (n = 3). Gel-like
226 samples (representative SH1/Ene2/Dz; **Supplementary Video_2**) are cut in square films and
227 the weights / dimensions are recorded for each sample to estimate the density values of tested
228 materials. Sample cuts (~1 mm thickness) are produced with a surgical blade and are placed
229 on PMMA slide centered between 2 UVA diodes (top and bottom of the sample). A PET
230 sheet is placed on the top of the sample, hand-pressed with the aid of glass microscope slide,
231 UVA diodes are turned ON, simultaneously to deliver the total dose of 20 J (counted together
232 from both sides; bottom through PMMA and top through glass + PET) to produce PMMA-
233 hybrid network-PET sandwich structure for lap shear adhesion test. Shear adhesion strength
234 is measured with Series Force Measurement System (Chatillon Force Measurement Products,
235 USA) equipped with 100 N loading cell (n = 7).

236 **2.7 Data processing**

237 All the calculations and graphs are produced in OriginPro software.

238

239 **3. RESULTS**

240 **3.1 Hybrid networks with diazirine-grafted polymer crosslinker: the scope**

241 The combination of polymers (**Figure 2; Table 1**) is hypothesized to form an instantaneous
242 hybrid gelation by: (i) single step curing with polychromatic light range of 320-500 nm
243 (thiol/alkyne/diazirine) or (ii) dual (2-step) crosslinking with monochromatic light
244 wavelengths at 405 nm (thiol/alkene; Step 1) and UVA (diazirine-to-carbene; Step 2; **Figure**
245 **1**). The overall design intent gives a light activated hybrid network for use as double sided

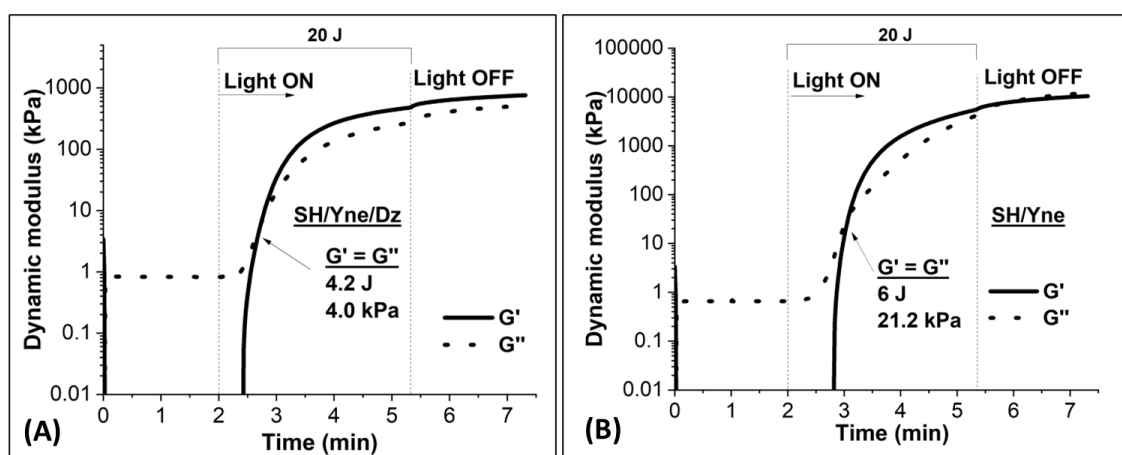
246 tissue adhesive patches. CaproGlu's liquid polymer nature creates the opportunity to dissolve
247 free radical and step growth polymerization monomers to create stimuli-based biomaterials.
248 Light irradiation at specific wavelengths can be selectively chosen to activate the monomers.
249 The following thiol/ene and thiol/yne monomers are common hydrogel precursors: 4-
250 functional thiol (SH), 2-functional alkene (Ene), 2-functional alkyne (Yne) and 2-functional
251 diazirine grafted polycaprolactone tetrol (CaproGlu; Dz). The exact mol ratios and respective
252 nomenclature are shown in **Table 1**; for example, the network "SH2/Ene2/Dz" is a 3-
253 component liquid mixture in the following molar ratio: PTHT/PEGDA/CaproGlu = 2/2.2/1
254 (structures are shown in **Figure 2**). Neat CaproGlu and 2-component hybrids (SH/Yne and
255 SH/Ene) are used as controls. Thiol/ene and thiol/yne crosslinked resins are selected for their
256 miscibility in CaproGlu and allow simultaneous or independent activation when doped with
257 visible light photoinitiators. Simultaneous activation is first evaluated with polychromatic
258 light in the range of 320-500 nm (2SH/2Yne/Dz; **Table 1**). Independent activation is
259 evaluated for the SH/Ene/CaproGlu hybrid elastomer by visible light (405 nm: thiol/ene
260 polymerization) [26], followed by CaproGlu activation with UVA light (365 nm: carbene-
261 based crosslinking).

262 The specific monomers (SH, Yne and Ene; **Figure 2**) are chosen as they are capable of
263 bioresorption via ester hydrolysis similar to polycaprolactone-based materials. Surface-
264 distributed diazirines are hypothesised to enable double sided adhesion by carbene insertion
265 upon UVA light activation. To investigate crosslinking kinetics, a custom photorheometer is
266 used to evaluate the real-time dynamic mechanical properties. One of the objectives is to find
267 compositions with low yield stress, also known as Bingham plastics (**Table 1**) that allow
268 substrate conformation for double sided adhesion. Structure-property relationships are
269 determined with respect to light energy exposure ($\text{J}\cdot\text{cm}^{-2}$; referred to as "J" further in text),
270 and tertiary ratios of the hybrid components. Qualitative analysis of surface chemistry is
271 evaluated by ATR-FTIR spectroscopy to observe chemical reactions of surface-exposed
272 functional groups before and after light activation. All hybrid networks are tested for their
273 peel strength when UVA-crosslinked between two hydrated collagen surfaces. Scanning
274 electron microscopy (SEM) evaluates the depth of CaproGlu activation through porous
275 morphologies and fundamental mechanical properties (lap shear adhesion strength and
276 toughness) are evaluated in regard to the cross-sectional depth of diazirine activation.

277

278 **3.2 Dynamic mechanical properties and crosslinking kinetics profiles are tuned by the**
279 **rule of mixtures between individual polymers**

280 Thiol/yne/Caproglu hybrid (SH2/Yne2/Dz; the exact mol ratios are shown in **Table 1**) is
281 activated with polychromatic light in UVA/visible range (320-500 nm; mercury lamp) for
282 simultaneous activation of CaproGlu (UVA) and the thiol/yne network (visible light). Storage
283 (G') and loss (G'') moduli are recorded as a function of time and irradiation dose (**Figure**
284 **3A**). Gelation ($G' = G''$) of SH2/Yne2/Dz hybrid network is reached at the dose of 4.2 J
285 (absorbed per cm^{-2} in all photorheometry experiments) which is almost three times higher
286 than gelation dose measured for pure CaproGlu (1.6 J; control-1) activated with mercury
287 lamp (320-500 nm; Supporting Information, **Figure S5**). The 2-component mixture SH/Yne
288 (control-2; **Table 1**) required a higher gelation dose of 6 J (**Figure 3B**).



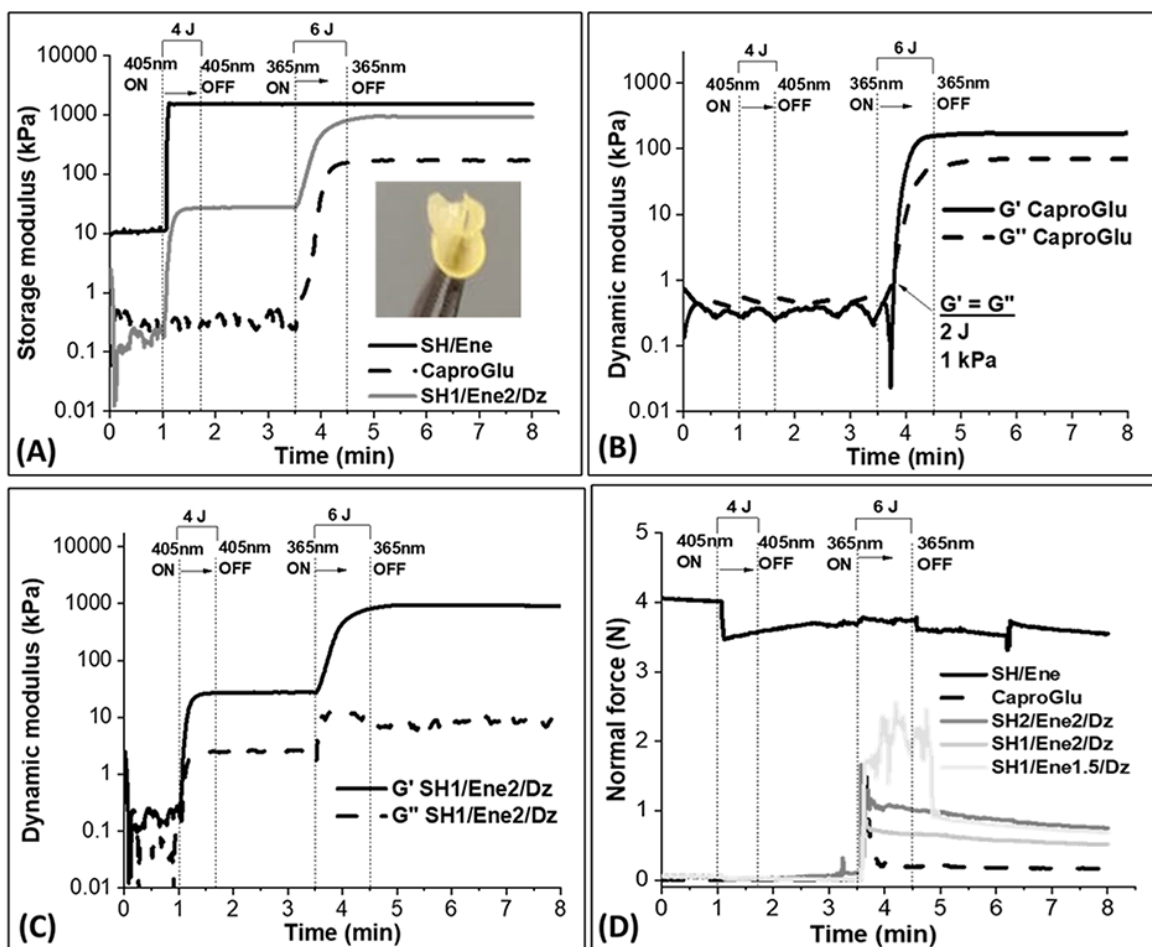
289 **Figure 3. Light activation of SH2/Yne2/Dz hybrid samples.** Liquid-to-solid transition of
290 hybrid networks analysed with photorheometry – dynamic change of storage (G') and loss
291 (G'') moduli with indicated gelation points ($G' = G''$) upon light activation (320-500 nm; 100
292 $\text{mW}\cdot\text{cm}^{-2}$) over measured time (bottom) and energy dose ($\text{J}\cdot\text{cm}^{-2}$; top): (A) 3-component
293 thiol/alkyne/CaproGlu hybrid: SH2/Yne2/Dz; (B) 2-component thiol/alkyne hybrid: SH/Yne
294 (control-2).
295

296
297 This result demonstrates that introduction of CaproGlu into the SH/Yne/Dz mixture results in
298 lowering the gelation point in simultaneous crosslinking process of thiol/yne and covalent
299 carbene insertion. Upon absorption of light at the total dose of 20 J, the hybrid 3-component
300 polymer network reaches dynamic modulus (G') value of 500 kPa (**Figure 3A**) that is an
301 order of magnitude lower than value reached for 2-component control-2 ($G' > 5 \text{ MPa}$; **Figure**

302 **3B**). Lower G' value likely results from emission of nitrogen upon diazirine photolysis and
303 formation of foam like structure [17, 18, 25]. Introduction of diazirine-grafted polymer into
304 thiol/yne reaction system results in 1-step reaction within seconds activated by polychromatic
305 mercury light (320-500 nm). This result expands the application of thiol/yne reaction that is
306 relevant in both bioorganic chemistry and polymer synthesis [27]. It should be noted that the
307 relatively high energy dose (20 J) is necessary to reach G' plateau for both SH₂/Yne₂/Dz
308 (**Figure 3**) and pure CaproGlu (**Figure S5**). This is a result of polychromatic light emitted
309 from mercury lamp (320-500 nm) where only the portion of the total absorbed light (320-390
310 nm) activates diazirine groups [17].

311 Thiol/ene precursors are selected for independent light activation investigations. These
312 precursors are available with similar molar mass (489 Da and 566 Da; **Figure 2**) to closely
313 align polymer and functional group molar ratios. Independent 2-step light activation of three
314 hybrid networks (**Table 1**) is evaluated by visible, followed by UVA activation. All 3-hybrid
315 network samples in **Table 1** with the two-step light activation are first sheared for 1 min
316 followed by irradiation with 405 nm light (Step-1). After 2 min no further changes in
317 modulus are observed and the sample is irradiated using a UVA diode (365 nm) with a 6 J
318 dose (Step-2; **Figure 4**). Light activation intervals are marked with dashed lines in **Figure 4**
319 and **Figure S6**. The representative evolution of G' for SH₁/Ene₂/Dz hybrid is compared to
320 pure CaproGlu (control-1) and 2-component diazirine-free SH/Ene mixture (control-3) as
321 shown in **Figure 4A**. Both SH/Ene (control-3) and SH₁/Ene₂/Dz hybrid show an increase in
322 G' values upon activation at 405 nm, indicating free-radical (thiol/ene) polymerization in the
323 presence of CaproGlu that remains unreactive until the UVA light is turned on.

324 According to rheometry data in **Figure 4A**, the rapid free-radical polymerization appears to
325 be faster in comparison to carbene-induced CaproGlu crosslinking (judging from the G' vs
326 irradiation time required to reach G' plateau). The 2-component control-3 (SH/Ene; no
327 CaproGlu) shows no change in G' upon UVA activation. Neat CaproGlu indicates liquid-to-
328 biorubber transition when activated either by polychromatic light (**Figure S5**) or
329 monochromatic UVA (365 nm) diode (**Figure 4B**). However, 3-component hybrid networks
330 (**Table 1**) undergo 2-step crosslinking without indication of gelation point (**Figure 4C**;
331 **Figure S6**). Note that pure CaproGlu takes 6 J UVA dose to reach G' value of ~170 kPa
332 (**Figure 4B**) consistent with previously published work on CaproGlu bioadhesive [17, 25].



333

334 **Figure 4.** 2-step energy directed crosslinking of liquid-to-solid hybrid network (3-component
 335 compositions are specified in **Table 1**) analysed with photoreometry by using different
 336 wavelengths: (A) representative dynamic change of storage moduli (G') of 3-component
 337 thiol/ene/CaproGlu hybrid network (SH1/Ene2/Dz) upon crosslinking at 405 nm (Step 1)
 338 followed by activation at 365 nm (Step 2) in comparison to 2-component thiol/ene (SH/Ene;
 339 control-3) and pure CaproGlu (control-1); the power of both diodes is adjusted to the total of
 340 10 J.cm^{-2} dose (diode power = 100 mW.cm^{-2}); (inset) SH1/Ene2/Dz transitioned into a
 341 flexible film after dual irradiation; (B) dynamic change of G' and loss modulus (G'') upon
 342 light irradiation recorded for pure CaproGlu with indicated gelation point ($G' = G''$); (C) G'
 343 and G'' change with irradiation energy recorded for SH1/Ene2/Dz; (D) normal force caused
 344 by the volume expansion of polymer networks upon light-activated crosslinking recorded for
 345 3-component hybrid networks compared to 2-component (SH/Ene; control-3) and pure
 346 CaproGlu (control-1). All data points are measured over time (bottom) and energy dose
 347 (J.cm^{-2} ; top)

348 Unlike controls that show no indication of crosslinking by either visible light (405 nm; pure
349 CaproGlu) or by UVA light (365 nm; 2-component SH/Ene), 3-component hybrid network
350 results in 2-step crosslinking process that is first activated by visible light (thiol/ene) followed
351 by UVA activation of diazirine to reach the maximum at 920 kPa recorded for SH1/Ene2/Dz
352 hybrid network (**Figure 4A and C**). Hybrid elastomeric films could be peeled off the
353 rheometer probe after a dual curing experiment as shown in **Fig. 4A-inset** (the rheometry
354 results are summarised in **Table S1**).

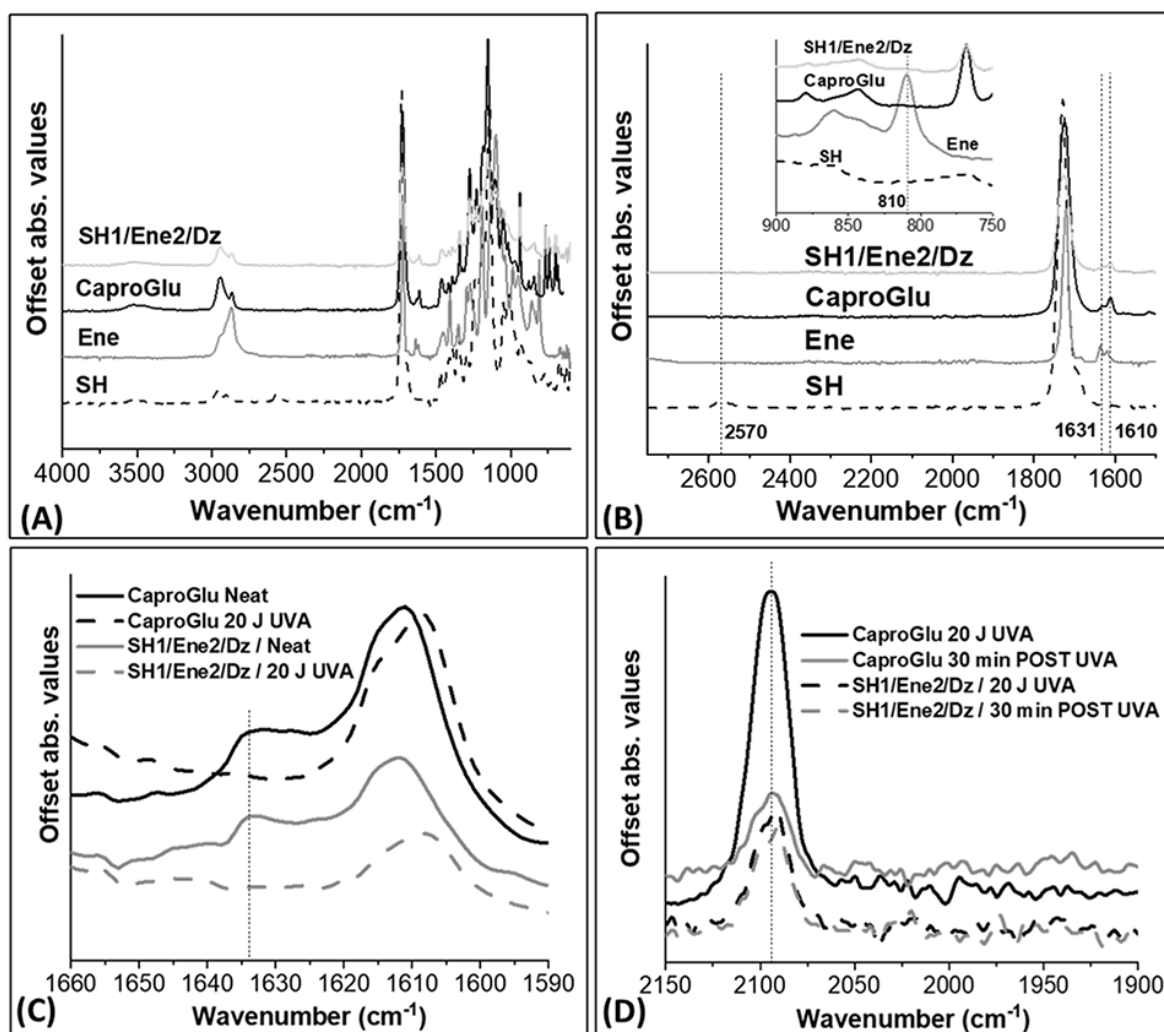
355 The photorheometer simultaneously assesses volumetric shrinkage by applying normal force
356 to maintain a predetermined sample thickness. The normal force to the rheometer probe is
357 monitored for both hybrid networks and controls 1-2 (pure CaproGlu and 2-component,
358 diazirine-free SH/Ene mixture, respectively) and results are shown in **Figure 4D**. Control-2
359 demonstrates a decrease of normal force with exposure to 100 mW.cm⁻² power 405 nm diode
360 within seconds. The SH/Ene molar ratio in control-2 (**Table 1**) is 1/2 for the highest density
361 of crosslinking between 4-functional thiol and 2-functional acrylate. A drop in normal force
362 is evidence for shrinkage and an increase signifies matrix expansion. Volume shrinking is
363 observed under visible light activation due to Michael addition and free radical crosslinking.
364 3-Component hybrid networks (**Table 1**) all resulted in sample volume shrinkage upon 405
365 nm activation (Step 1) as evident from drop in normal force (see **Figure S7**). CaproGlu
366 shows no change in normal force during Step 1 light activation (405 nm; 4 J; **Figure S7**)
367 suggesting the inert nature of diazirine groups towards visible light (405 nm). Under UVA
368 light exposure, diazirine photolysis releases molecular nitrogen as a byproduct that in turn
369 causes foaming [17, 25]. Volume expansion is evident in both pure CaproGlu (control-1) and
370 3-component hybrid samples (**Figure 4D**). This further supports the hypothesis of hybrid
371 network crosslinking with independent light wavelengths.

372 The hybrid networks are observed to spontaneously solidify over 24 h (no UVA activation)
373 when exposed to laboratory ambient environment, which may be due to visible light
374 activation (**Figure S2**). Note that SH1/E1.5/Dz hybrid network (refer to **Table 1** for exact
375 mol ratio) results in viscoelastic solids (i.e. Bingham plastic) material (**Figure S1**). The
376 elastomeric hybrid composition can be cut into solid, double sided adhesive polymer
377 (network SH1Ene2/Dz; **Table 1**; **Supplementary Video_1**) and forms a solid material after
378 24 h exposure to ambient light; this formulation has a ~1/1 ratio thiol/ene (**Table 1**). The
379 absence of gelation points in hybrid networks (**Figure 4C**; **Figure S6**) is possibly a
380 consequence of immediate reaction upon mixing under ambient light condition as the

381 photorheometry analysis is performed within 30 min after sample preparation. The absence of
382 gelation points (recorded 30 min after mixing) are consistent with the macroscopic
383 appearance of hybrid networks that form either solid gels or Bingham plastic materials even
384 without direct irradiation by 405 nm light diode (**Figure S1**). Note that stoichiometric
385 SH/Ene ratio in SH1/Ene2/Dz (4-arm thiol and 2-arm acrylate; **Figure 2**) results in highest G'
386 = 28 kPa upon 405 nm activation in comparison to SH2/Ene2/Dz (16 kPa) and
387 SH1/Ene1.5/Dz (7 kPa) where unreacted thiol acts as plasticizer (**Figure 4; Figure S6; Table**
388 **S1**). Although the highest relative concentration of diazirines is in SH1/Ene1.5/Dz, the
389 stoichiometric thiol/acrylate ratio (SH1/Ene2/Dz) results in the highest recorded G' after
390 second activation step with UVA (920 kPa) compared to 410 kPa and 630 kPa recorded for
391 SH2/Ene2/Dz and SH1/Ene1.5/Dz respectively (**Figure 4; Figure S6**). Carbene reacts both at
392 the surface and within the bulk of materials, depth limited by macromolecule scattering. The
393 unreacted thiol within the hybrid networks might act as carbene scavenger thus reducing the
394 extent of surface reaction with both base and the probe of photorheometer, that in turn results
395 in relatively low modulus.

396 **3.3 FTIR spectroscopy identifies covalent crosslinks within hybrid networks**

397 FTIR spectroscopic analysis is performed to qualitatively observe the depletion of reactive
398 functional groups upon photoreactions (**Figure 5**), namely: out of plane $-C=C-$ stretch
399 vibrations at 810 cm^{-1} (2-Ene) [21, 28], S-H absorption peaks at 2570 cm^{-1} (4-SH) [29],
400 diazirine ring at 1634 cm^{-1} [25, 30] and diazoalkane intermediate peaks at 2092 cm^{-1} [25, 31].
401 The network SH1/Ene2/Dz (the exact molar ratio is shown in **Table 1**) is chosen for this
402 experiment to prove the hypothesis that under visible light only thiol reacts to completion
403 with acrylate while diazirine groups remain unreacted. **Figure 5A** shows full spectra of both
404 hybrid SH1/Ene2/Dz and neat components (no UVA activation) while **Figure 5B** is a
405 magnified region used in this analysis. Note that the peaks at $1640\text{--}1610\text{ cm}^{-1}$ of Ene
406 (assigned to $-C=C-$ from acrylate) overlap with diazirine ($-N=N-$; 1630 cm^{-1}) and $-C-N$
407 (1610 cm^{-1}) [25] peaks from CaproGlu and therefore could not be used to observe reaction of
408 acrylates [32]. For that reason, the peak at 810 cm^{-1} is selected to analyse Ene (acrylate)
409 reaction within hybrid matrix (**Figure 5B-inset**). Both thiol (2570 cm^{-1}) and acrylate (810 cm^{-1})
410 disappear in SH1/Ene2/Dz sample after photocuring by ambient light with estimated
411 degree of Ene conversion of ~80% even before activation with UVA light (**Figure S8**).



412

413 **Figure 5.** FTIR spectral regions recorded for representative 3-component thiol/ene/CaproGlu
 414 hybrid network (SH1/Ene2/Dz) and pure polymer components (structures and nomenclature
 415 of individual component are shown in **Figure 1**): (A) full FTIR spectral region (no UVA);
 416 (B) diazirine (1631 cm^{-1} ; CaproGlu and SH1/Ene2/Dz), -C-N (1610 cm^{-1}), -S-H (2570 cm^{-1});
 417 pure 4-functional thiol: SH) peaks; (inset) -C=C- stretch vibration at 809 cm^{-1} from
 418 diacrylate groups (Ene; no UVA); (C) disappearance of diazirine peak (1634 cm^{-1} ; dashed
 419 line) upon UVA activation; (D) diazoalkane (2094 cm^{-1}) persistence over the period of 24 h
 420 upon UVA activation of 3-component hybrid network (SH1/Ene2/Dz) and pure CaproGlu.

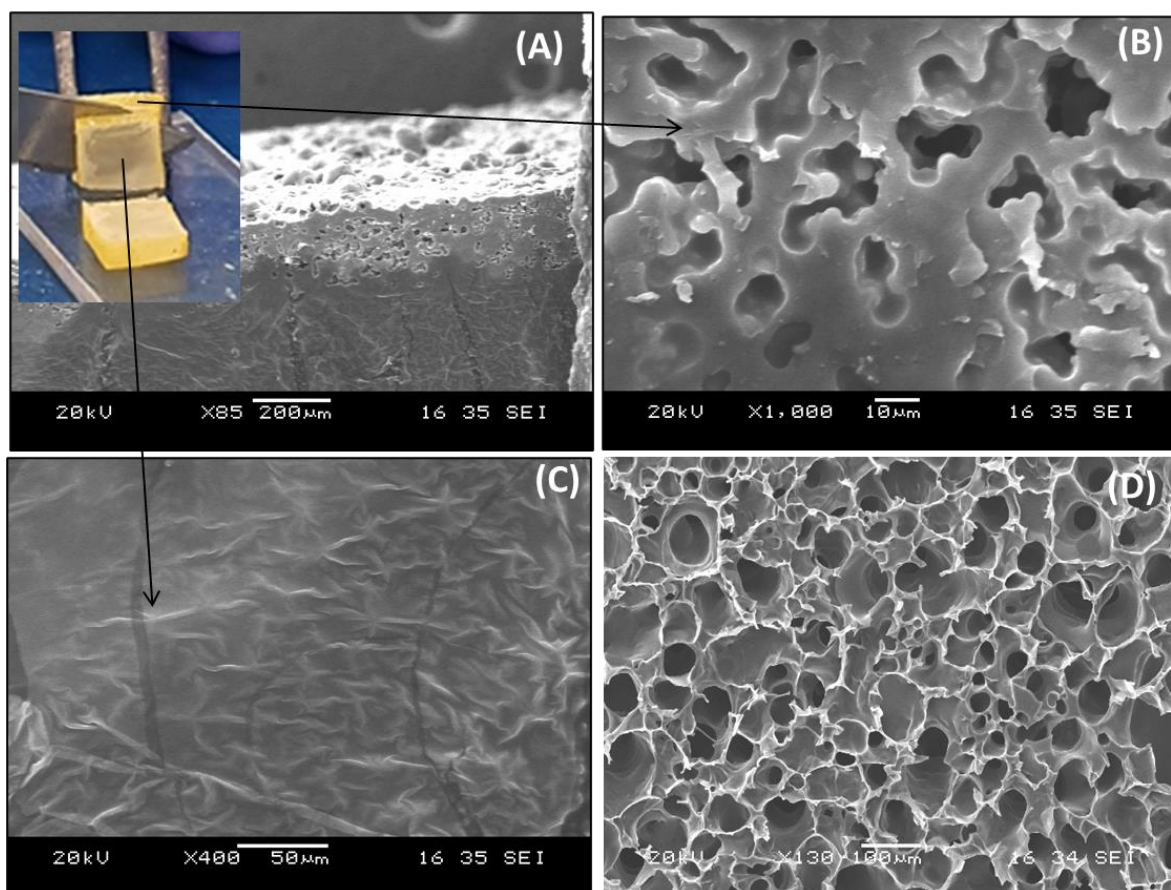
421

422 Upon UVA activation, diazirine undergoes photolysis as recorded from disappearance of
 423 -N=N- peak at 1630 cm^{-1} (**Figure 5C**). Two products are possible from diazirine photolysis:
 424 carbene and diazoalkane. The semi-stable nature of the diazoalkane is demonstrated by the
 425 presence of 2090 cm^{-1} peak absorbance of both SH1/Ene2/Dz hybrid and neat CaproGlu

426 (control) 30 min post-UVA activation (**Figure 5D**). Previously published FTIR results
427 provide the evidence that the diazoalkane decay kinetics is dependent on the functional
428 groups adjacent to diazine [33]. The intermolecular environment (in this case SH/Ene
429 mixture) is likely to influence the fate of diazoalkane, however this requires dedicated
430 kinetics study in future research. It is hypothesized that the adhesion to solid surfaces of 3-
431 component hybrid network is facilitated by the fraction of the diazine groups that are
432 distributed at the hybrid surface after the first crosslinking step. From theoretical estimation
433 (according to molar ratio in **Table 1**) the SH1/Ene2/Dz network contains 70 nmol.cm⁻² of
434 diazine groups for the sample thickness of 1 μm (the density of this particular network is 1.1
435 g.cm⁻³; **Table S2**). Indeed, diazine groups are detected in ATR-FTIR experiment (**Figure**
436 **5C**) with penetration depth of ATR probe to be ~100 nm [34]. With evidence that diazine
437 surface groups remain unreacted, double sided adhesives are possible.

438 **3.4 UVA activation of diazine component results in porous surface micro-morphology** 439 **detected by SEM**

440 As indicated by the double sided adhesive nature of the 3-component SH1/Ene2/Dz hybrid
441 network (**Table 1**), UVA irradiation activates the sample surface causing covalent insertion
442 of carbenes onto solid polymer interfaces (**Supplementary Videos 1 and 2**). SEM analysis of
443 cross-section (**Figure 6**) is performed to examine the penetration depth of diazine activation
444 visually observed by the colour change (from white opaque to yellow; **Figure 4A-inset**).
445 Arrows pointing out from **Figure 6A-inset** indicate different parts of SH1/Ene2/Dz cross-
446 section (surface **Figure 6B** and bulk **Figure 6C**) analysed with SEM. UVA activation of
447 CaproGlu causes evolution of molecular nitrogen that in turn results in porous crosslinked
448 matrix [25]. From **Figure 6A-B**, the porous matrix is formed at the surface of the hybrid
449 network with estimated penetration depth of molecular nitrogen in the range of 100-150 μm
450 while the middle portion of the sample (**Figure 6C**) shows micro-wrinkled morphology,
451 characteristic for elastomeric surfaces [35]. The pore size generated by molecular nitrogen
452 (diazine photolysis) is in the range of 5-10 μm (**Figure 6B**), 10x smaller than neat
453 CaproGlu with pore size of 50-100 μm (**Figure 6D**).



454

455 **Figure 6.** SEM images of cross-section of 3-component thiol/ene/CaproGlu hybrid polymer
 456 network after 10 J.cm^{-2} of UVA activation indicating the outer porous and inner
 457 homogeneous morphology of UVA activated sample - 2 parts of the sample, surface and bulk
 458 (inset photography) are indicated by arrows: (A-C) SH1/Ene2/Dz; (D) pure CaproGlu
 459 (control-1) activated with 10 J.cm^{-2} of UVA (magnification bar: $100 \mu\text{m}$).

460 Decrease of pore size is a direct consequence of material properties – unlike the crosslinked
 461 hybrid network that results in a semi-solid material, liquid (neat) CaproGlu results in lower
 462 stress that inhibits nitrogen bubble expansion. Knowing the penetration depth of CaproGlu
 463 crosslinking within the SH1/Ene2/Dz hybrid network ($100\text{-}150 \mu\text{m}$; **Figure 6A**) attention
 464 should be given to the rheometry base-gap probe that is set for $100 \mu\text{m}$, and therefore
 465 dynamic moduli (G') in **Figure 4** and **Figure S6** are representative of complete diazirine
 466 (CaproGlu) crosslinking within the total volume of analysed hybrid network sample (**Figure**
 467 **4A-inset**) as confirmed by SEM. Elastomeric wrinkled morphology [36] in the bulk of
 468 SH1/Ene2/Dz hybrid is in line with visual observation of the material (**Supplementary**
 469 **Video_1**).

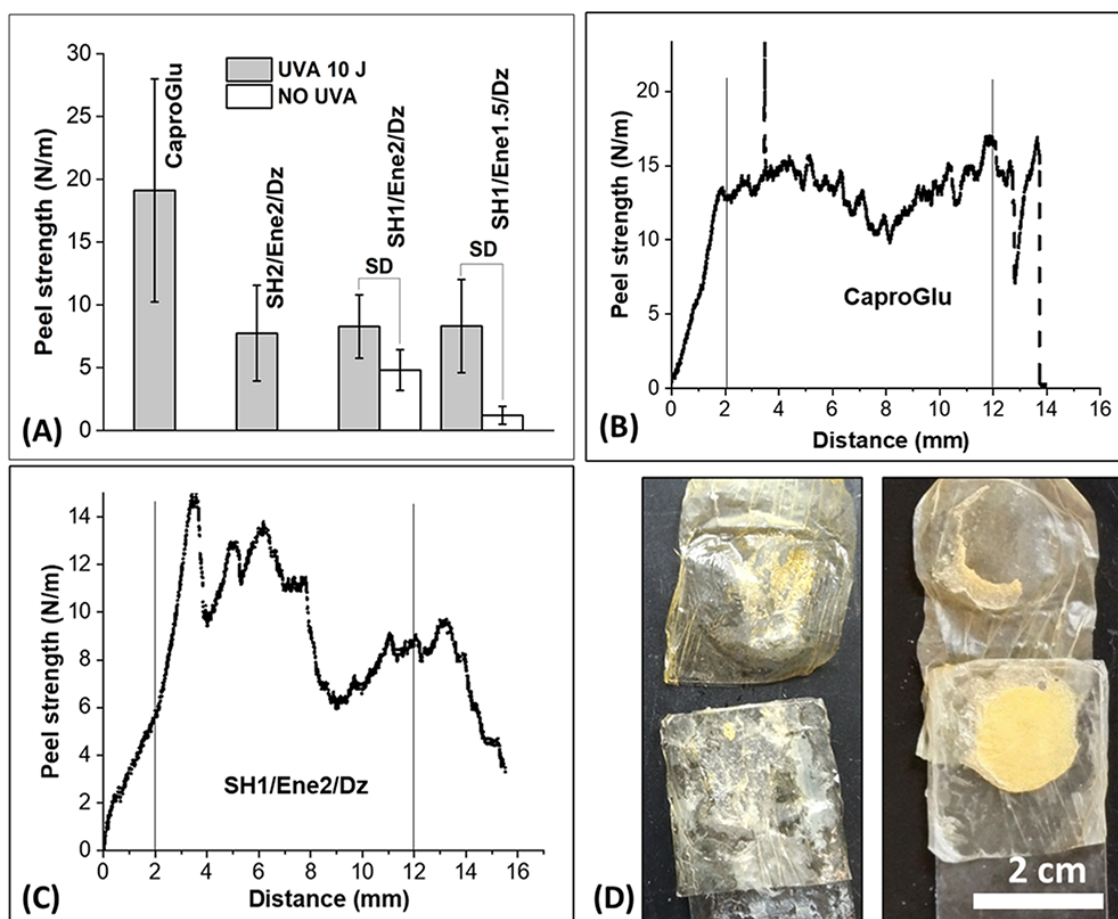
470 Crosslinked SH1/Ene2/Dz (Step 1; 405 nm) does not allow pore expansion deeper and larger
471 than measured by SEM, however, future work could demonstrate that the pore size might be
472 controlled by the following parameters: (1) concentration of grafted diazirine and molecular
473 weight of polycaprolactone polyol; (2) CaproGlu concentration within composite (hybrid)
474 network; and (3) crosslinking density activated with visible light, prior to UVA activation.
475 Furthermore, diazirine can be activated with longer wavelength at 445 nm (with the aid of
476 photocatalyst) [18] that will possibly allow light-activated crosslinking deeper than 150 μm .

477 **3.5 Double sided adhesive hybrid network properties**

478 Hybrid network SH1/Ene2/Dz (**Table 1**) has demonstrated light sensitivity in both visible
479 light (405 nm; $G' = 28$ kPa at 4 J dose) and UVA (365 nm; $G' = 920$ kPa at 6 J dose)
480 resulting in the highest dynamic moduli in comparison to other hybrid networks (**Figure 4**;
481 **Table S1**). Predetermined SH/Ene ratio (1/2) results in complete thiol/ene reaction (as
482 evident from FTIR spectroscopic analysis; **Figure 5B**) forming a gel polymer network after
483 activation by visible light at low energy dose (4 J; **Figure 4A**). Rheometry results
484 demonstrate that CaproGlu was unaffected by visible light and could be activated
485 independently – visible light activation of SH1/Ene2/Dz hybrid allows mm thick specimens
486 to be setup even in the presence of CaproGlu (**Supplementary Videos 1 and 2**). Diazirines
487 are known to convert into carbene upon UVA activation that in turn results in unselective
488 crosslinking, both polymer bulk (intermolecular) and at any proximate surface (i.e. polymer,
489 tissue proteins) [17]. Peel strength experiment is performed for hybrid networks where the
490 samples (**Figure S3**) are placed between two hydrated collagen surfaces (**Figure S4**) and
491 subsequently activated with UVA light from both sides of the “sandwich” structure with the
492 total dose of 20 J (10 J delivered through each collagen film). The obtained results are
493 compared to the following controls: 1) neat CaproGlu before and after UVA activation; 2)
494 two-component blend SH/Ene (without CaproGlu) previously crosslinked under ambient
495 light (**Figure S3**) and subsequently irradiated with 20 J of UVA light through collagen sheets;
496 3) hybrid polymer networks fixed between two collagen films without UVA activation
497 (**Figure 7**).

498

499



500

501 **Figure 7.** Peel adhesion strength measured for HPN samples (and pure CaproGlu used as
 502 control) activated through hydrated collagen surfaces with 2 UVA diodes – each side of all
 503 samples absorbed the UVA energy = 10 J.cm^{-2} (total absorbed dose = 20 J.cm^{-2}): (A) peel
 504 strength measured for HPN samples compared to CaproGlu control ($n = 3$; ANOVA: $p < 0.05$;
 505 SD = statistically different); (B and C) representative peel strength profiles collected for pure
 506 CaproGlu and SH1/Ene2/Dz respectively (data between 2 vertical lines is used to calculate
 507 average peel strength for each sample – 2 mm after the beginning of the test and 2 mm before
 508 adhesion failure); (D) representative photographs of collagen strips with crosslinked
 509 CaproGlu (left) and SH1/Ene2/Dz (right) samples after peel strength experiment.

510

511 All tested hybrid networks resulted in peel adhesion strength (after UVA activation) of 8 ± 3
 512 N/m with a relatively large standard deviation and without significant difference between
 513 samples (**Figure 7A**). All the raw data used to calculate values in **Figure 7A** are shown in
 514 **Figures S9-11**. This result corresponds with photorheological properties where no change in
 515 dynamic modulus could be recorded upon UVA activation without the presence of diazirine

516 component (**Figure 4**). Hybrid polymer networks SH1/Ene2/Dz and SH1/Ene1.5/Dz show
517 adhesion when pressed between hydrated collagen sheets with the aid of paper clips (**Figures**
518 **S4 and S11**). However, the values of 5 ± 2 N/m and 1.2 ± 0.7 N/m (SH1/Ene2/Dz and
519 SH1/Ene1.5/Dz respectively) are significantly lower than peel adhesion strength recorded
520 after UVA activation (**Figure 7A**). Both neat CaproGlu and two-component network
521 (SH2/Ene2) controls do not show any adhesion that could be recorded without UVA
522 irradiation. Together with FTIR analysis (**Figure 5**), this result supports the hypothesis that
523 the diazirine groups are present at the hybrid network surface and result in adhesion when
524 activated with UVA light at the hydrated biopolymer interface (collagen). Neat CaproGlu
525 results in significantly higher peel strength after UVA activation (19 ± 9 kPa) when compared
526 to tested hybrid networks (**Figure 7A**). This result is expected because diazirine groups in gel
527 networks (**Figure S3**) are diluted and thus cause lower peel strength than crosslinked
528 CaproGlu. Furthermore, during the peel experiment, the fracture of crosslinked polymer
529 propagates evenly for CaproGlu as the fracture strength is distributed over the entire sample
530 volume (**Figure 7B; Figure S9**). Representative peel adhesion data for hybrid polymer
531 network (SH1/Ene2/Dz; **Figure 7C**) shows peak and trough indicating larger strain fracture
532 toughness. CaproGlu fails cohesively during peel test [17, 18], unlike in crosslinked hybrid
533 networks that demonstrate adhesive failure due to diazirine dilution (representative
534 photographs are shown in **Figure 7D**). Increased toughness by formation of a hybrid network
535 matrix correlates with rheology results (**Figure 4**) that indicate crosslinked matrix upon
536 thiol/ene reaction activated by visible light (Step-1; **Figure1**).

537 Cohesive nature of CaproGlu adhesive is consistent with previously published results on pure
538 CaproGlu used in artery anastomosis aided with polycaprolactone (PCL) mesh tape [17]. The
539 biorubber nature of hybrid network (**Supplementary Video_2**) allows compliance with soft
540 tissues and potentially could prevent implant failure and injuries due to biomechanical
541 mismatch. The elastic nature of crosslinked hybrid network is further investigated in lap shear
542 adhesion test to polymer surfaces that resulted in ultimate adhesion strength of 160 ± 50 kPa
543 (representative SH1/Ene2/Dz; **Figure S12A-B**). The elastic behaviour is also evident from
544 modulus vs strain diagram (**Figure S12C**) calculated as the first derivative of stress vs strain
545 function. The modulus value increases from 140 kPa to the maximum value of 197 kPa at
546 0.42 (mm/mm) strain and sustains strain > 0.8 (marked with dashed arrow in **Figure S12C**).
547 The strain energy density (toughness) of the hybrid network is measured to be 80 ± 40 kJ.m⁻³
548 (**Figure S12D**) for the samples of ~ 2 mm thickness (**Figure S12B-inset; Table S2**). The

549 toughness of the hybrid network is an order of magnitude lower than the toughness value
550 reported for thin CaproGlu film (~20 μm) activated at biological surfaces (~20 $\text{MJ}\cdot\text{m}^{-3}$
551 collagen/CaproGlu/porcine skin) [18]. This result indicates that UVA activation is spatially
552 limited by UVA penetration depth through hybrid polymer network since all measured
553 samples failed cohesively (**Figure S13C**). The measured lap shear adhesion strength of
554 hybrid network is comparable to pure CaproGlu (170 ± 10 kPa; **Figure S13**). Unlike the peel
555 test performed with irregular, hydrated collagen films that results in adhesive failure (**Figure**
556 **7**), the hybrid network failed cohesively when crosslinked on flat, fully transparent polymer
557 surfaces (PET and PMMA; **Figures S12** and **S13**). The diazine adhesion is stronger than
558 thiol/ene crosslinked network as evident by repetitive cohesive failure in lap shear adhesion
559 tests. Due to the cohesive nature of the double sided adhesive hybrid network, the diazine
560 adhesion strength remains unknown. It is evident that the diazine surface adhesion is
561 stronger than thiol/ene cohesive strength that always fails first.

562

563 **4. DISCUSSION**

564 Hybrid polymer blends that incorporate independent light activated crosslinking mechanisms
565 have been explored for the first time. Hybrid composites of thiol/ene and carbene-based
566 biomaterials serve as a model system to explore how viscous formulations can be rapidly
567 photocured into tough bioelastomers. The design requires liquid precursors that are miscible
568 yet remain relatively inactive. Liquid mixtures of CaproGlu, ester alkyne, PEG-based alkene,
569 and multi-arm thiol were miscible and chemically inert (**Figure 2**). Both alkenes and alkynes
570 react with thiols via radical polymerization [37] and require a visible light-activated initiator
571 – for independent activation between the two polymer networks [26]. CaproGlu is inert to
572 free-radical or visible light exposure, a considerable advantage for gamma sterilization and
573 ambient shelf stability [17]. Upon photoactivation, CaproGlu emits nitrogen, resulting in a
574 porous biorubber in both neat CaproGlu and hybrid polymer networks presented in this work.
575 The surface porosity of implanted biomaterials is known to accelerate tissue resorption while
576 the tunable elastic modulus of hybrid polymer network is possible in the range of 400-950
577 kPa in broad wavelength light activation (320-500 nm) and focused activation by visible light
578 (405 nm) followed by crosslinking and surface adhesion activated by UVA (365 nm) light.
579 Diacrylate/tetrathiol system has also shown crosslinking under ambient light. However, the 2-

580 step crosslinking might be possible with other multifunctional alkenes to produce systems
581 with higher stability and more controlled photocuring mechanism [38].

582 The solvent-free hybrid network material allows for a flexible liquid-to-elastomer transition
583 through various optical stimulation profiles. Thiol/ene crosslinking proceeds in the presence
584 of inert and transparent CaproGlu, resulting in dynamic modulus transition from liquid to ~30
585 kPa (modulus) gel upon activation with visible light (405 nm). Subsequent exposure to UVA
586 (365 nm), activates non-specific carbene insertion. The hybrid networks display a relatively
587 broad range of shear modulus from 10-800 kPa, which can be easily tuned through both
588 optical exposure and precursor molar ratio. The modulus near the surface (100 μm depth) of
589 the hybrid network may allow modulus gradients to obtain matching elasticity profiles [39].
590 Apart from the potential control over depth of CaproGlu crosslinking, the porous surface of
591 hybrid network (pore size: ~10 μm) is beneficial for tissue engineering strategies where
592 neovascularization/cell migration is facilitated through interfacial porous structure of
593 implanted scaffolds [40].

594 Due to the homogeneous mixing of all three components, diazirine groups are present at the
595 surface of the hybrid network. Hybrid polymer networks result in adhesion to both dry
596 substrates and wet collagen surfaces. Surface diazirine groups (from CaproGlu component)
597 resulted in carbene covalent insertion onto solid polymers (PMMA and PET). This covalent
598 insertion adheres hybrid network to polymers by reaching ~160 kPa of adhesion strength,
599 limited by cohesive failure after applied lap shear adhesion stress. The penetration depth of
600 diazirine photolysis was found to be in the range of 100-150 μm while the diazirines
601 embedded within the network presumably remain unreacted. Diazirines are known to degrade
602 into ketones, alcohols, ethers or other chemical groups [41]. Both kinetics of diazirine
603 degradation (photolysis) and the nature of degradation products are dependent on the
604 chemical environment [33, 41]. However, the results in this paper indicate possibility of
605 double adhesive tape with 100 μm thickness where all diazirine groups are reacted, both
606 within the bulk of material and at the substrate interface.

607 Low molar mass diazomethane precursors require precautions due to their explosive nature
608 [42]. However, trifluoromethyl diazirine-based compounds (that lead to carbene and
609 diazoalkane intermediates) are known for their stability with reported crosslinking activation
610 that initiates at 110 $^{\circ}\text{C}$ [43]. CaproGlu synthesis reaction is stable (no detectable exothermic
611 effect) at 40 $^{\circ}\text{C}$ with exceptional shelf stability even after 25 kGy gamma sterilization, ergo

612 the aryl-diazirine is inert to free-radical exposure and most nucleophilic functional groups—a
613 claim few crosslinking groups hold [17, 25]. Apart from the stability of the diazirine used for
614 polymer grafting, polycaprolactone tetrol (PCLT) precursors are available in food-grade
615 quality and therefore present few risks towards medical devices. PCLT belongs to the
616 platform of PCL-based biodegradable materials that are known to undergo ester hydrolysis
617 and physiological elimination of degradation products goes through well-defined metabolic
618 reactions such as citric acid and fatty acid pathways [69]. Polymerization of
619 thiol/ene/CaproGlu hybrid networks, initiated by exposure to gamma irradiation, may be
620 exploited for selective activation or depletion of acrylates without need of photoinitiators.
621 CaproGlu would remain intact and to provide the same on-demand crosslinking / adhesion
622 characteristics. In addition, CaproGlu can be activated with visible light (445 nm) when
623 mixed with photocatalysts, which opens up possibilities for dual crosslinking activated by
624 two distinct visible wavelengths [18]. Unlike NHS-grafted bioadhesives [13], grafting of
625 carbene-generating diazirine onto liquid polycaprolactone polyols resulted in bioadhesive
626 with non-discriminated covalent insertion to both hydrated biologically-derived surfaces and
627 solid synthetic polymers [17]. CaproGlu is one example of the emerging carbene-based
628 bioadhesive platform. The liquid polymer requires no refrigeration or rehydration and can be
629 processed into ready-to-use implantable medical devices that are stable to gamma
630 sterilization, a key attribute for industrial scale-up. CaproGlu has displayed little to no
631 inflammation tested *in vivo* [17] and low-risk skin sensitization *in vitro* (OECD-regulated
632 genotoxicity and sensitization tests) [25].

633 Thiol/ene crosslinking is available for many different polymer systems, including acrylate-
634 grafted polysaccharides and PEG macromolecules with a wide range of molecular weights
635 and geometries [44]. In particular, PEG diacrylate is known commercial photopolymer
636 precursor, available in a wide range of molecular weights [45]. PEG-based polymer networks
637 are known for their application in hybrid bioprinting technology [46] and the ester bonds aid
638 miscibility within CaproGlu, allowing solvent-free mixing. In addition, polycaprolactone polyols
639 (triols and tetrols) are readily available with molecular weights between 300 and 2000 Da,
640 allowing a library of materials with various viscoelastic properties [47]. Hybrid systems
641 mentioned herein could be extended beyond hydrophobic PCLTs. Amphiphilic formulations
642 could be designed with dendrimers [48-50]. This extends diazirine activation method to
643 applied voltage (Voltaglue) providing that the crosslinkers are dispersed in conductive
644 medium. The choice of initiator would determine the wavelength of light used for free-radical

645 activation. For example, UV-active Igracure 2929 can be replaced with Eosin Y activated
646 with visible light (405 nm) to crosslink acrylate-thiol systems [51]. However, it is also known
647 that photoinitiators pose risks as toxic leachates [52]. Hybrid networks based on
648 thiol/ene/carbene may eliminate photoinitiators through gamma initiation. Future work will
649 explore this process to form sterile double sided adhesives.

650

651 **5. CONCLUSION**

652 Diazirine-grafted polycaprolactone (CaproGlu) can be mixed with acrylates, thiols and
653 alkynes to form hybrid polymer networks with a high degree of control over material
654 properties. The dual curing macromolecular systems are independently activated by visible
655 light followed by mild UVA activation. When activated by visible light, polymer hybrid only
656 partially crosslinks into gel-like material and remains reactive for subsequent adhesion onto
657 solid surfaces by on-demand UVA activation of surface diazirine groups. Unselective
658 crosslinking of diazirine-generated carbene enables chemical anchoring of double sided
659 adhesive gels to any types of solid substrates without surface pre-treatment that is normally
660 required for formation of interfacial heterogenous chemical bonding. These attributes of
661 CaproGlu crosslinking formulation demonstrate multifunctional nature, both intermolecular
662 and interfacial crosslinking, that would lead towards biomedical applications with careful
663 selection of network components without need of solvents or photoinitiators.

664 **CRedit authorship contribution statement**

665 Ivan Djordjevic: Investigation, Formal analysis, Data curation, Writing – original draft.
666 Gautama Wicaksono: Data curation, Methodology. Manisha Singh: Data curation,
667 Methodology. Elizabeth G. Ellis: Data curation, Methodology. Maher A. Alraddadi: Data
668 curation, Methodology. Andrew P. Dove: Conceptualization, Supervision, Writing – review
669 & editing. Terry W.J. Steele: Conceptualization, Formal analysis, Supervision, Writing –
670 review & editing, Funding acquisition.

671 **Declaration of Competing Interest**

672 T.W.J. Steele and I. Djordjevic are co-inventors of the following IP: Hygroscopic,
673 Crosslinking Coatings and Bioadhesives; PCT/SG2018/050452. Authors declare no
674 competing interests. CaproGlu is an abbreviation for this technology and is not trade marked.

675

676 **Acknowledgements**

677 This work is funded by Institute of Advanced Studies Birmingham Visiting Fellowship,
678 ‘Strong Elastomeric Bioadhesives Towards Tendon Repair’; Ministry of Education Tier 1
679 Grant RT07/20: Fiber-optic orthopaedic implants for bone-implant adhesion, Ministry of
680 Education Tier 2 Grant (MOE2018-T2-2-114): CaproGlu, Double sided wet-tissue adhesives,
681 NTUitive POC (Gap) Fund NGF/2018/05: Aesthetic Applications of CaproGlu Bioadhesives,
682 and A*STAR IAF PP Grant (H19/01/a0/0II9): CathoGlu Bioadhesives-preventing catheter
683 extravasation and skin infections.

684

685 **References:**

- 686 [1] S. Czarnecki, T. Rossow, S. Seiffert, Hybrid Polymer-Network Hydrogels with Tunable
687 Mechanical Response, *Polymers* 8(3) (2016) 82.
- 688 [2] M.A. Haque, T. Kurokawa, J.P. Gong, Super tough double network hydrogels and their
689 application as biomaterials, *Polymer* 53(9) (2012) 1805-1822.
- 690 [3] J.P. Gong, Why are double network hydrogels so tough?, *Soft Matter* 6(12) (2010) 2583-
691 2590.
- 692 [4] H. Yuk, T. Zhang, S. Lin, G.A. Parada, X. Zhao, Tough bonding of hydrogels to diverse
693 non-porous surfaces, *Nature materials* 15(2) (2016) 190-196.
- 694 [5] J. Deng, Z. Dai, J. Yan, M. Sandru, E. Sandru, R.J. Spontak, L. Deng, Facile and solvent-
695 free fabrication of PEG-based membranes with interpenetrating networks for CO₂ separation,
696 *Journal of Membrane Science* 570-571 (2019) 455-463.
- 697 [6] M. Sangermano, W. Carbonaro, G. Malucelli, A. Priola, UV-Cured Interpenetrating
698 Acrylic-Epoxy Polymer Networks: Preparation and Characterization, *Macromolecular*
699 *Materials and Engineering* 293(6) (2008) 515-520.
- 700 [7] V. Granskog, O.C.J. Andrén, Y. Cai, M. González-Granillo, L. Felländer-Tsai, H. von
701 Holst, L.-A. Haldosen, M. Malkoch, Linear Dendritic Block Copolymers as Promising
702 Biomaterials for the Manufacturing of Soft Tissue Adhesive Patches Using Visible Light
703 Initiated Thiol–Ene Coupling Chemistry, *Advanced Functional Materials* 25(42) (2015)
704 6596-6605.
- 705 [8] A.H.C. Anthis, X. Hu, M.T. Matter, A.L. Neuer, K. Wei, A.A. Schlegel, F.H.L. Starsich,
706 I.K. Herrmann, Chemically Stable, Strongly Adhesive Sealant Patch for Intestinal
707 Anastomotic Leakage Prevention, *Advanced Functional Materials* 31(16) (2021) 2007099.
- 708 [9] L. Zeng, J. He, Y. Cao, J. Wang, Z. Qiao, X. Jiang, L. Hou, J. Zhang, Tissue-adhesive and
709 highly mechanical double-network hydrogel for cryopreservation and sustained release of
710 anti-cancer drugs, *Smart Materials in Medicine* 2 (2021) 229-236.
- 711 [10] H.Y. Jung, P. Le Thi, K.-H. HwangBo, J.W. Bae, K.D. Park, Tunable and high tissue
712 adhesive properties of injectable chitosan based hydrogels through polymer architecture
713 modulation, *Carbohydrate Polymers* 261 (2021) 117810.
- 714 [11] S. Nam, D. Mooney, Polymeric Tissue Adhesives, *Chemical Reviews* (2021).
- 715 [12] X. Chen, H. Yuk, J. Wu, C.S. Nabzdyk, X. Zhao, Instant tough bioadhesive with
716 triggerable benign detachment, *Proceedings of the National Academy of Sciences* 117(27)
717 (2020) 15497-15503.

718 [13] H. Yuk, C.E. Varela, C.S. Nabzdyk, X. Mao, R.F. Padera, E.T. Roche, X. Zhao, Dry
719 double-sided tape for adhesion of wet tissues and devices, *Nature* 575(7781) (2019) 169-174.

720 [14] M.H. Turabee, T. Thambi, D.S. Lee, Development of an Injectable Tissue Adhesive
721 Hybrid Hydrogel for Growth Factor-Free Tissue Integration in Advanced Wound
722 Regeneration, *ACS Applied Bio Materials* 2(6) (2019) 2500-2510.

723 [15] A. Shagan, W. Zhang, M. Mehta, S. Levi, D.S. Kohane, B. Mizrahi, Hot Glue Gun
724 Releasing Biocompatible Tissue Adhesive, *Advanced Functional Materials* 30(18) (2020)
725 1900998.

726 [16] N. Oliva, S. Shitreet, E. Abraham, B. Stanley, E.R. Edelman, N. Artzi, Natural Tissue
727 Microenvironmental Conditions Modulate Adhesive Material Performance, *Langmuir* 28(43)
728 (2012) 15402-15409.

729 [17] I. Djordjevic, O. Pokhonenko, A.H. Shah, G. Wicaksono, L. Blancafort, J.V. Hanna, S.J.
730 Page, H.S. Nanda, C.B. Ong, S.R. Chung, A.Y.H. Chin, D. McGrouther, M.M. Choudhury,
731 F. Li, J.S. Teo, L.S. Lee, T.W.J. Steele, CaproGlu: Multifunctional tissue adhesive platform,
732 *Biomaterials* 260 (2020) 120215.

733 [18] I. Djordjevic, G. Wicaksono, I. Šolić, J. Singh, T.S. Kaku, S. Lim, E.W.J. Ang, L.
734 Blancafort, T.W.J. Steele, Rapid Activation of Diazirine Biomaterials with the Blue Light
735 Photocatalyst, *ACS Applied Materials & Interfaces* (2021).

736 [19] L.J. Macdougall, V.X. Truong, A.P. Dove, Efficient In Situ Nucleophilic Thiol-yne
737 Click Chemistry for the Synthesis of Strong Hydrogel Materials with Tunable Properties,
738 *ACS Macro Letters* 6(2) (2017) 93-97.

739 [20] C.E. Hoyle, C.N. Bowman, Thiol-ene click chemistry, *Angewandte Chemie*
740 *International Edition* 49(9) (2010) 1540-1573.

741 [21] A.E. Rydholm, C.N. Bowman, K.S. Anseth, Degradable thiol-acrylate photopolymers:
742 polymerization and degradation behavior of an in situ forming biomaterial, *Biomaterials*
743 26(22) (2005) 4495-4506.

744 [22] P.M. Kharkar, M.S. Rehmann, K.M. Skeens, E. Maverakis, A.M. Kloxin, Thiol-ene
745 click hydrogels for therapeutic delivery, *ACS biomaterials science & engineering* 2(2) (2016)
746 165-179.

747 [23] Y. Dong, A.O. Saeed, W. Hassan, C. Keigher, Y. Zheng, H. Tai, A. Pandit, W. Wang,
748 "One-step" Preparation of Thiol-Ene Clickable PEG-Based Thermoresponsive
749 Hyperbranched Copolymer for In Situ Crosslinking Hybrid Hydrogel, *Macromolecular rapid*
750 *communications* 33(2) (2012) 120-126.

751 [24] K. Jin, N. Wilmot, W.H. Heath, J.M. Torkelson, Phase-Separated Thiol-Epoxy-Acrylate
752 Hybrid Polymer Networks with Controlled Cross-Link Density Synthesized by Simultaneous
753 Thiol-Acrylate and Thiol-Epoxy Click Reactions, *Macromolecules* 49(11) (2016) 4115-
754 4123.

755 [25] I. Djordjevic, G. Wicaksono, I. Solic, T.W. Steele, In Vitro Biocompatibility of
756 Diazirine-Grafted Biomaterials, *Macromolecular Rapid Communications* 41(21) (2020)
757 2000235.

758 [26] B. Steyrer, P. Neubauer, R. Liska, J. Stampfl, Visible light photoinitiator for 3D-printing
759 of tough methacrylate resins, *Materials* 10(12) (2017) 1445.

760 [27] J.C. Worch, C.J. Stubbs, M.J. Price, A.P. Dove, Click Nucleophilic Conjugate Additions
761 to Activated Alkynes: Exploring Thiol-yne, Amino-yne, and Hydroxyl-yne Reactions from
762 (Bio)Organic to Polymer Chemistry, *Chemical Reviews* 121(12) (2021) 6744-6776.

763 [28] L. Maleki, U. Edlund, A.-C. Albertsson, Synthesis of full interpenetrating hemicellulose
764 hydrogel networks, *Carbohydrate polymers* 170 (2017) 254-263.

765 [29] N.B. Cramer, J.P. Scott, C.N. Bowman, Photopolymerizations of thiol-ene polymers
766 without photoinitiators, *Macromolecules* 35(14) (2002) 5361-5365.

767 [30] A. Gambi, M. Winnewisser, J.J. Christiansen, The infrared spectrum of diazirine:
768 Rovibrational analysis of the ν_3 fundamental, *Journal of Molecular Spectroscopy* 98(2)
769 (1983) 413-424.

770 [31] R. Cataliotti, A. Poletti, G. Paliani, A. Foffani, Infrared Spectrum and Vibrational
771 Assignment of Diazocyclopentadiene-h4 and-d4, *Zeitschrift für Naturforschung B* 27(8)
772 (1972) 875-878.

773 [32] M.-A. Tehfe, J. Lalevée, S. Telitel, E. Contal, F.d.r. Dumur, D. Gignes, D. Bertin, M.
774 Nechab, B. Graff, F. Morlet-Savary, Polyaromatic structures as organo-photoinitiator
775 catalysts for efficient visible light induced dual radical/cationic photopolymerization and
776 interpenetrated polymer networks synthesis, *Macromolecules* 45(11) (2012) 4454-4460.

777 [33] I. Djordjevic, G. Wicaksono, I. Solic, T.W.J. Steele, Diazoalkane decay kinetics from
778 UVA-active protein labelling molecules: Trifluoromethyl phenyl diazirines, *Results in*
779 *Chemistry* 2 (2020) 100066.

780 [34] P. Luan, G.S. Oehrlein, Characterization of Ultrathin Polymer Films Using p-Polarized
781 ATR-FTIR and Its Comparison with XPS, *Langmuir* 35(12) (2019) 4270-4277.

782 [35] I. Djordjevic, N. Choudhury, N. Dutta, S. Kumar, Poly(octanediol-co-(citric acid)-co-
783 (sebacic acid)) elastomers: novel bio-elastomers for tissue engineering, *Polymer International*
784 60 (2011) 333-343.

785 [36] I. Djordjevic, N.R. Choudhury, N.K. Dutta, S. Kumar, E.J. Szili, D.A. Steele,
786 Polyoctanediol Citrate/Sebacate Bioelastomer Films: Surface Morphology, Chemistry and
787 Functionality, *Journal of Biomaterials Science, Polymer Edition* 21(2) (2010) 237-251.

788 [37] O. Tüürüç, M.A.R. Meier, A novel polymerization approach via thiol-yne addition,
789 *Journal of Polymer Science Part A: Polymer Chemistry* 50(9) (2012) 1689-1695.

790 [38] M. Sahin, S. Ayalur-Karunakaran, J. Manhart, M. Wolfahrt, W. Kern, S. Schlögl, Thiol-
791 Ene versus Binary Thiol-Acrylate Chemistry: Material Properties and Network
792 Characteristics of Photopolymers *Advanced Engineering Materials* 19(4) (2017) 1600620.

793 [39] H. Saraf, K.T. Ramesh, A.M. Lennon, A.C. Merkle, J.C. Roberts, Mechanical properties
794 of soft human tissues under dynamic loading, *Journal of Biomechanics* 40(9) (2007) 1960-
795 1967.

796 [40] Q.L. Loh, C. Choong, Three-Dimensional Scaffolds for Tissue Engineering
797 Applications: Role of Porosity and Pore Size, *Tissue Engineering Part B: Reviews* 19(6)
798 (2013) 485-502.

799 [41] A.B. Kumar, J.D. Tipton, R. Manetsch, 3-Trifluoromethyl-3-aryldiazirine photolabels
800 with enhanced ambient light stability, *Chemical Communications* 52(13) (2016) 2729-2732.

801 [42] S.P. Green, K.M. Wheelhouse, A.D. Payne, J.P. Hallett, P.W. Miller, J.A. Bull, Thermal
802 Stability and Explosive Hazard Assessment of Diazo Compounds and Diazo Transfer
803 Reagents, *Organic Process Research & Development* 24(1) (2020) 67-84.

804 [43] M.L. Lepage, C. Simhadri, C. Liu, M. Takaffoli, L. Bi, B. Crawford, A.S. Milani, J.E.
805 Wulff, A broadly applicable cross-linker for aliphatic polymers containing C-H bonds,
806 *Science* 366(6467) (2019) 875-878.

807 [44] G.M. Cruise, D.S. Scharp, J.A. Hubbell, Characterization of permeability and network
808 structure of interfacially photopolymerized poly(ethylene glycol) diacrylate hydrogels,
809 *Biomaterials* 19(14) (1998) 1287-1294.

810 [45] A. Bagheri, J. Jin, Photopolymerization in 3D Printing, *ACS Applied Polymer Materials*
811 1(4) (2019) 593-611.

812 [46] W. Li, L.S. Mille, J.A. Robledo, T. Uribe, V. Huerta, Y.S. Zhang, Recent Advances in
813 Formulating and Processing Biomaterial Inks for Vat Polymerization-Based 3D Printing,
814 *Advanced Healthcare Materials* 9(15) (2020) 2000156.

815 [47] W.J. Steele, Terry ; Djordjevic, I. , Hygroscopic, Crosslinking Coatings and
816 Bioadhesives, <https://patentscope.wipo.int/search/en/detail.jsf?docId=WO2019050479>
817 PCT/SG2018/050452 (2019).
818 [48] M. Singh, C.S. Yin, S.J. Page, Y. Liu, G. Wicaksono, R. Pujar, S.K. Choudhary, G.U.
819 Kulkarni, J. Chen, J.V. Hanna, R.D. Webster, T.W.J. Steele, Synergistic Voltagelue Adhesive
820 Mechanisms with Alternating Electric Fields, *Chemistry of Materials* 32(6) (2020) 2440-
821 2449.
822 [49] J. Ping, F. Gao, J.L. Chen, R.D. Webster, T.W. Steele, Adhesive curing through low-
823 voltage activation, *Nature communications* 6(1) (2015) 1-9.
824 [50] G. Feng, I. Djordjevic, V. Mogal, R. O'Rorke, O. Pokhonenko, T.W.J. Steele, Elastic
825 Light Tunable Tissue Adhesive Dendrimers, *Macromolecular Bioscience* 16(7) (2016) 1072-
826 1082.
827 [51] A. Fu, K. Gwon, M. Kim, G. Tae, J.A. Kornfield, Visible-light-initiated thiol–acrylate
828 photopolymerization of heparin-based hydrogels, *Biomacromolecules* 16(2) (2015) 497-506.
829 [52] R. Taschner, P. Gauss, P. Knaack, R. Liska, Biocompatible photoinitiators based on
830 poly- α -ketoesters, *Journal of Polymer Science* 58(2) (2020) 242-253.

831